Developmental Biology 377 (2013) 55–66

Contents lists available at SciVerse ScienceDirect

Developmental Biology

journal homepage: www.elsevier.com/locate/developmentalbiology

Aberrant Wnt signalling and cellular over-proliferation in a novel mouse model of Meckel–Gruber syndrome

Gabrielle Wheway [a], Zakia Abdelhamed [a,b], Subaashini Natarajan [a], Carmel Toomes [a], Chris Inglehearn [a], Colin A. Johnson [a,*]

[a] Section of Ophthalmology and Neurosciences, Leeds Institute of Molecular Medicine, Beckett Street, The University of Leeds, Leeds, LS9 7 TF, UK
[b] Department of Anatomy and Embryology, Faculty of Medicine, Al-Azhar University, Cairo, Egypt

ARTICLE INFO

Article history:
Received 17 October 2012
Received in revised form
6 February 2013
Accepted 13 February 2013
Available online 27 February 2013

Keywords:
Cilia
Ciliopathies
Wnt signalling
Proliferation
Embryonic development

ABSTRACT

Meckel–Gruber syndrome (MKS) is an embryonic lethal ciliopathy resulting from mutations in genes encoding proteins localising to the primary cilium. Mutations in the basal body protein MKS1 account for 7% of cases of MKS. The condition affects the development of multiple organs, including brain, kidney and skeleton. Here we present a novel Mks1$^{tm1a(EUCOMM)Wtsi}$ knockout mouse which accurately recapitulates the human condition, consistently developing pre-axial polydactyly, complex posterior fossa defects (including the Dandy–Walker malformation), and renal cystic dysplasia. TOPFlash Wnt reporter assays in mouse embryonic fibroblasts (MEFs) showed general de-regulated high levels of canonical Wnt/β-catenin signalling in Mks1$^{-/-}$ cells. In addition to these signalling defects, we also observed ectopic high proliferation in the brain and kidney of mutant animals at mid- to late-gestation. The specific role of Mks1 in regulating cell proliferation was confirmed in *Mks1* siRNA knockdown experiments which showed increased levels of proliferation after knockdown, an effect not seen after knockdown of other ciliopathy genes. We suggest that this is a result of the de-regulation of multiple signalling pathways (Wnt, mTOR and Hh) in the absence of functional Mks1. This novel model system offers insights into the role of MKS1 in Wnt signalling and proliferation, and the impact of deregulation of these processes on brain and kidney development in MKS, as well as expanding our understanding of the role of Mks1 in multiple signalling pathways.

Introduction

Meckel–Gruber syndrome (MKS) is a perinatal lethal developmental condition considered to be the most frequent syndromic cause of neural tube defects (Simpson et al., 1991). The condition is characterised by the classic 'triad' of occipital encephalocele, polycystic kidneys and post-axial polydactyly. These features are almost always accompanied by ductal proliferation in the portal area of the liver (a hepatic developmental defect), which is considered by some to be an additional diagnostic criterion of MKS. Central nervous system (CNS) defects commonly seen in MKS include occipital encephalocele, rhombic roof dysgenesis and prosencephalic dysgenesis which may include olfactory bulb dysgenesis, optic nerve hypoplasia, agenesis of the corpus callosum, or total holoprosencephaly. These features suggest an underlying defect in ventral induction of the developing CNS by the prechordal mesoderm (Ahdabbarmada and Claassen, 1990). In addition to these, other CNS features sometimes seen in MKS include microcephaly, cerebellar hypoplasia or total anencephaly, and midline defects such as absence of the lateral ventricles (Paetau et al., 1985). The Dandy–Walker malformation (Dandy and Blackfan, 1914; Taggart and Walker, 1942) which comprises cystic swelling of the fourth ventricle to fill the posterior fossa and dysgenesis/agenesis of the cerebellar vermis is also sometimes observed (Genuardi et al., 1993; Herriot et al., 1991; Murray et al., 1985; Summers and Donnenfeld, 1995). The fourth ventricle is filled with cerebrospinal fluid (CSF) and the swelling seen in Dandy–Walker malformation is often associated with hydrocephaly, another occasional feature of MKS (Lowry et al., 1983). Other occasional features include shortening and bowing of the long bones, talipes, genital malformations, microphthalmia and other ocular defects, congenital heart defects, cleft lip and palate (Salonen, 1984; Sugiura et al., 1996) tongue lobulations and tumours (Moerman et al., 1982b) and situs defects including polysplenia/asplenia (Moerman et al., 1982a) and situs inversus (Rapola and Salonen, 1985).

Ten genes have been identified which, when mutated, cause MKS. All of these causative genes encode proteins which localise to the primary cilium or basal body of the cell. The cilium is a microtubule structure found on the ventral surface of epithelial

* Corresponding author. Fax: +44 0113 343 8603.
E-mail address: c.johnson@leeds.ac.uk (C.A. Johnson).

0012-1606/$ - see front matter © 2013 Elsevier Inc. All rights reserved.
http://dx.doi.org/10.1016/j.ydbio.2013.02.015

cells. Defects in primary cilia have been found to be associated with many human diseases, and cilia are now known to have important roles in mechanosensation (Nauli et al., 2003; Praetorius and Spring, 2001), in signal transduction in the Hedgehog, Wnt and PDGFRα signalling pathways (Davis et al., 2006) and in the establishment of left–right asymmetry (Nonaka et al., 1998). Cilia therefore have essential roles throughout embryogenesis and development, and the clinical consequences of the aberrant development or function of primary cilia are a group of inherited human disorders known as the ciliopathies, of which MKS is the most severe (Adams et al., 2008).

Mutations in *MKS1* account for around 7% of all MKS cases and around 70% of Finnish MKS cases due to a genetic founder effect (Khaddour et al., 2007). The MKS1 gene encodes a 559 amino acid B9-domain containing protein which localises to the basal body of mammalian cells (Kyttala et al., 2006) to regulate ciliogenesis in association with meckelin and two other B9-domain containing proteins, B9D1 and B9D2 (Dawe et al., 2007a; Williams et al., 2008). It is believed that the B9 domain is required for centriolar localisation of MKS1 and subsequent ciliogenesis (Cui et al., 2011), and that Tectonic-1 (TCTN1) plays a role in transporting MKS1 (and other MKS proteins) to the transition zone between the basal body and ciliary axoneme (Garcia-Gonzalo et al., 2011). MKS1 has also been shown to interact with TCTN2 and CC2D2A (MKS6), in a module regulating Sonic Hedgehog (SHH) signalling (Sang et al., 2011), and the role of Mks1 in Hedgehog signalling has been well-characterised in mouse models. The *kerouac* (*krc*) mutant model of Mks1 exhibited classic Shh mutant phenotypes, including polydactyly, lung hypoplasia and supraoccipital hypoplasia. Genetic analyses showed that in the mouse, Mks1 acts upstream of Patched, and loss of Mks1 in Mks^{krc} mutant mice led to Shh patterning defects in the neural tube and limb. Mutant embryos showed broader domains of low-level Shh signalling and reduction in high-level Shh signalling (Weatherbee et al., 2009). $Mks1^{del64\text{-}323}$ mutant mice also exhibited polydactyly, polycystic kidneys, situs defects, congenital heart abnormalities and craniofacial malformations. Shh signalling defects were also observed, with an increase in signalling due to lower Gli3-repressor expression (Cui et al., 2011).

The possible involvement of MKS1 in other signalling pathways, including the Wnt pathway, has not been investigated in previous mouse models of MKS type 1, despite the manifestation of defects that are consistent with a defect in planar cell polarity (PCP) and non-canonical Wnt signalling (Cui et al., 2011). Nor has Wnt signalling been investigated in other animal systems recapitulating MKS type 1, such as *mks1* morphant zebrafish. Line-labelling of blastomeres in *mks1* morphant zebrafish shows a convergent extension defect, typical of PCP defects, but this has not been investigated at the molecular level (Leitch et al., 2008). Here, we describe the phenotype of a novel $Mks1^{tm1a(EUCOMM)Wtsi}$ knockout mouse and investigate the contribution of Wnt signalling defects and cell over-proliferation to disease phenotypes in the developing brain and kidney of this ciliopathy model.

Materials and methods

Animals

The animal studies described in this paper were carried out under the guidance issued by the Medical Research Council in *Responsibility in the Use of Animals for Medical Research* (July 1993) in accordance with UK Home Office regulations under the Project Licence no. PPL40/3349. B6.129P2-$Mks1^{tm1a(EUCOMM)Wtsi}$ heterozygous knock-out mice were derived from a line generated by the Wellcome Trust Sanger Institute and made available from MRC Harwell through the European Mutant Mouse Archive 〈http://www.emmanet.org/〉 (strain number EM:05429). The $Mks1^{tm1a}$ allele was generated by the European Mouse Mutagenesis Programme using a 'knockout-first' gene targeting cassette. $Mks1^{+/-}$ heterozygous mice were obtained and back-crossed onto a C57B6 line for five generations. Genotyping was done by PCR on DNA extracted from tail tips or the yolk sac of E10.5–E11.5 embryos, or tail or ear biopsies of older embryos and adult mice, respectively.

Timed-matings

Female mice in matings were checked for vaginal plugs every morning, and the gestational stage was estimated from the time of a positive plug+0.5 days.

Reverse-transcriptase PCR (RT-PCR)

Total RNA was obtained from MEFs and homogenised cryogenically-ground hind limbs using TRIzol reagent (Invitrogen), following the manufacturer's instructions, and cDNA was synthesised using Moloney murine leukaemia virus reverse transcriptase (m-MLV RT) (Invitrogen) and random primers (Invitrogen). Exons upstream (exon 4) and downstream (exon 6) of the mutation cassette insertion were amplified using primers complementary to flanking exons in mutant, wild-type and heterozygote MEFs and analysed by gel electrophoresis and direct sequencing. Genomic DNA was included as a control.

Quantitative RT-PCR

Each quantitative PCR reaction mixture of 25 μl contained 12.5 μl of SYBR Green PCR master mix (Applied Biosystems), 300 nM each of forward (F) and reverse (R) primers and 2 μl of 10 times diluted cDNA. Primer sequences are as follows: *Ptch1* (Patched 1) F: 5′ GCTGTGGCTGAGAGCGAAGT, R: 5′ AAATATGAGGAGACCACAACCA; *Shh* F: 5′ AAAGCTGACCCCTTTAGCCTA, R: 5′ TTCGGAGTTTCTTGTGATCTTC; *Axin2* F: 5′ GCAGTGTGAAGGCCAATGG, R: GCAGGCGGTG GGTTCTC; *Actb* (β-actin) F: GCTTCTTTGCAGCTCCTTCGT, R: AGCGCAGCGATATCGTCAT. Reactions were carried out in triplicate using the ABI Prism 7500 system (Applied Biosystems). The cycling conditions included initial denaturation for 2 min at 50 °C, 10 min at 95 °C, followed by amplification for 40 cycles of 15 s each at 95 °C and a final extension of 1 min at 60 °C. The average C_t values of the samples were normalised to values for β-actin. Fold-difference in expression of the different genes in the mutant embryos was calculated relative to their expression in wild-type or heterozygous littermates using the $\Delta\Delta C_t$ method.

Preparation of tissue sections, histology and immunohistochemistry

Mouse embryos or dissected tissues were either left unfixed and embedded in optimal cutting temperature embedding medium (OCT) (ThermoFisher Scientific) for cryopreservation or fixed in 4% (w/v) para-formaldehyde, dehydrated in 70% ethanol and embedded in paraffin wax. Thin sections (5 μm) of paraffin-embedded samples were cut onto "Superfrost Plus" slides (VWR International Ltd.) using a microtome. Sections of samples in OCT were cut using a Cryostat. Paraffin-embedded sections were deparaffinised and rehydrated by standard methods. Sections were stained with haematoxylin and eosin (BDH Chemicals Ltd.) for 2 min, then dehydrated in ethanol, cleared in xylene and mounted in DPX. For IHC, epitope recovery was obtained by boiling in 1 mM EDTA pH8.0, for 2 min using a pressure cooker, followed by 30 min of cooling. Blocking and application of primary antibodies: mouse anti-Ki67 (BD Biosciences) 1:200; rabbit anti-active caspase 3 (Abcam) 1:100, was as described (Dawe et al., 2007b). Appropriate HRP-conjugated secondary

antibodies (Dako Inc.) were used at 1:20000 dilution. Sections were developed in "Sigma Fast" 3,3′-diaminobenzidine (DAB) with $CoCl_2$ enhancer and counterstained with Mayer's haematoxylin (Sigma-Aldrich Co. Ltd.).

Immunofluorescent staining

MEFs grown on coverslips and cryosections were fixed in ice-cold methanol, blocked with 1% non-fat milk/PBS and immunostained with mouse anti-acetylated alpha tubulin (Sigma) 1:1000; rabbit anti-gamma tubulin (Abcam) 1:500; rabbit anti-β-catenin (Cell Signaling Technology) 1:200. After washing with PBS, cells were incubated with AlexaFluor 488- or 568-conjugated secondary antibodies (Sigma) 1:1000 and DAPI 1:1000 and mounted using Mowiol mounting medium.

Skeletal and cartilage staining preparations

Alizarin red staining of bone and alcian blue staining of cartilage was carried out essentially as described in Nagy et al. (2003).

Cells

Mouse inner medullary collecting duct (IMCD3) cells were grown in Dulbecco's minimum essential medium (DMEM)/Ham's F12 supplemented with 10% foetal calf serum at 37 °C/5% CO_2. The derivation and culture of mouse embryonic fibroblasts (MEFs) has been described previously (Xu, 2001). MEFs were grown in DMEM/Ham's F12 supplemented with 10% foetal calf serum and 1% penicillin streptomycin at 37 °C/5% CO_2.

Reverse transfection of siRNAs, high throughput staining and high content imaging

Reverse transfections were carried out in Opti-MEM using 50 nM final concentration of 4 pooled siRNA duplexes (Dharmacon) and 0.2 μl RNAiMAX (Invitrogen) per well in 96-well "ViewPlate" (PerkinElmer Inc.). 8×10^3 IMDC3 cells, suspended in OPTI-MEM were plated per well and then incubated for 72 h at 37 °C/5% CO_2. For IMCD3 cells reverse transfected with siRNAs, cells were washed three times with PBS, fixed with ice cold methanol and incubated for 5 min. at −20 °C. Afterwards cells were washed, blocked and processed for immunofluorescence by standard procedures. Primary cilia were detected with mouse anti-acetylated-α-tubulin diluted at x1000, and goat anti-mouse IgG AlexaFluor488-conjugated secondary antibody (at x2000 dilution). Cells were counterstained with DAPI and TOTO3 (both at x5000 dilution) (Invitrogen Inc.). Images were acquired on an Operetta high content screening system (Perkin–Elmer Inc.) using Harmony software (Perkin–Elmer). Images were analysed with Columbus software (Perkin–Elmer) to count cilia and cell numbers. Analysis scripts are available on request. Further description of image acquisition and analysis can be found in Elmehdawi et al., 2013.

Preparation of protein extracts from tissues and cells (MEFs, IMCD3s)

Protein was extracted from frozen tissue samples by grinding the tissue with a pestle and mortar frozen with liquid nitrogen and kept on dry ice. Ground tissue was heated to 95 °C for 15 min in 4% SDS/200 mM β-mercaptoethanol/20% glycerol solution. The extract was cleared by centrifugation at $10{,}000 \times g$ for 15 min. Protein was extracted from cultured cells by washing the cells with cold PBS three times and lysing with 1% NP40/150 mM NaCl/10% glycerol/2 mM EDTA lysis buffer containing complete protease inhibitor cocktail for 15 min at 4 °C. Lysates were cleared by centrifugation at $10{,}000 \times g$ for 15 min.

Western blotting

Protein samples were prepared in 2x SDS loading buffer (4% SDS/200 mM β-mercaptoethanol/20% glycerol/bromophenol blue) and loaded onto 4–12% Bis-Tris polyacrylamide gels and run at 130 V for 1 h. Proteins were transferred to PVDF membrane at 30 V for 90 min. Membranes were blocked in 5% non-fat milk/PBST for 1 h and incubated with primary antibodies (mouse anti-Gli3N 6F5 (Wen et al., 2010) 1:500; rabbit anti-β-catenin (Cell Signaling Technology) 1:1000; rabbit anti-MKS1 (Sigma) 1:500; anti-β-actin (Abcam) 1:5000) for 3 h. After three PBST washes, membranes were incubated with HRP-conjugated secondary antibodies (Dako) and visualised using Femto substrate (Pierce) on a BioRad ChemiDoc system using Image Lab software.

Canonical Wnt activity (TOPFlash) luciferase assays

1×10^5 MEFs were seeded per well in 24-well cell culture plates 24 h before transfection so that cells were at 80% confluency at the time of transfection. Cells were co-transfected with 0.5 μg TOPFlash firefly luciferase construct (or FOPFlash, as a negative control) and 0.05 μg of pRL-TK internal control *Renilla* luciferase reporter construct (Promega Corp) using Lipofectamine 2000 (Invitrogen Inc.) in Opti-MEM, according to the manufacturer's instructions and as described previously (Dawe et al., 2009). Cells were treated with Wnt3a- or Wnt5a-conditioned media for 16 h before the cells were harvested (Willert et al., 2003). Luciferase activities were assayed with the Dual-Luciferase Reporter Assay system (Promega Corp.) on a Mithras LB940 (Berthold Technologies Inc.) luminometer. Raw readings were normalised with *Renilla* luciferase values, and the results reported are from at least four independent biological replicates.

Statistical analyses

Normal distribution of data (TOPFlash activities, cilia length measurements) was confirmed using the Kolmogorov–Smirnov test (GraphPad Software). Pairwise comparisons were analysed with Student's two-tailed *t*-test using InStat (GraphPad Software). Results reported are from at least three independent biological replicates, unless otherwise stated. Error bars on bar graphs indicate s.e.m. The statistical significance of pairwise comparisons shown on bar graphs are indicated by: # not significant, $^{*}p < 0.05$, $^{**}p < 0.01$, $^{***}p < 0.001$, and $^{****}p < 0.0001$. For cell populations, a minimum of 150 cells were counted from 10 separate fields of view.

Results

Out of 183 embryos obtained through timed-mating, 40 showed mutant phenotypes, consistent with a normal Mendelian monogenic inheritance of a recessive trait. All of the animals with a mutant phenotype had homozygous insertion of the targeted mutation *tm1a* cassette in *Mks1*. An additional five embryos that were resorbed and not suitable for phenotypic analysis also had the $Mks1^{-/-}$ genotype. Reverse transcriptase PCR (RT-PCR) and Sanger sequencing analysis of *Mks1* cDNA from $Mks1^{-/-}$ mutant embryos confirmed insertion of the *tm1a* cassette into intron 4 of *Mks1*, upstream of exon 5, a critical exon present in all known transcripts of *Mks1* (Fig. 1a) causing an out-of-frame insertion (data not shown). The predicted effect of the insertion was to cause nonsense-mediated decay of transcript, reducing levels of

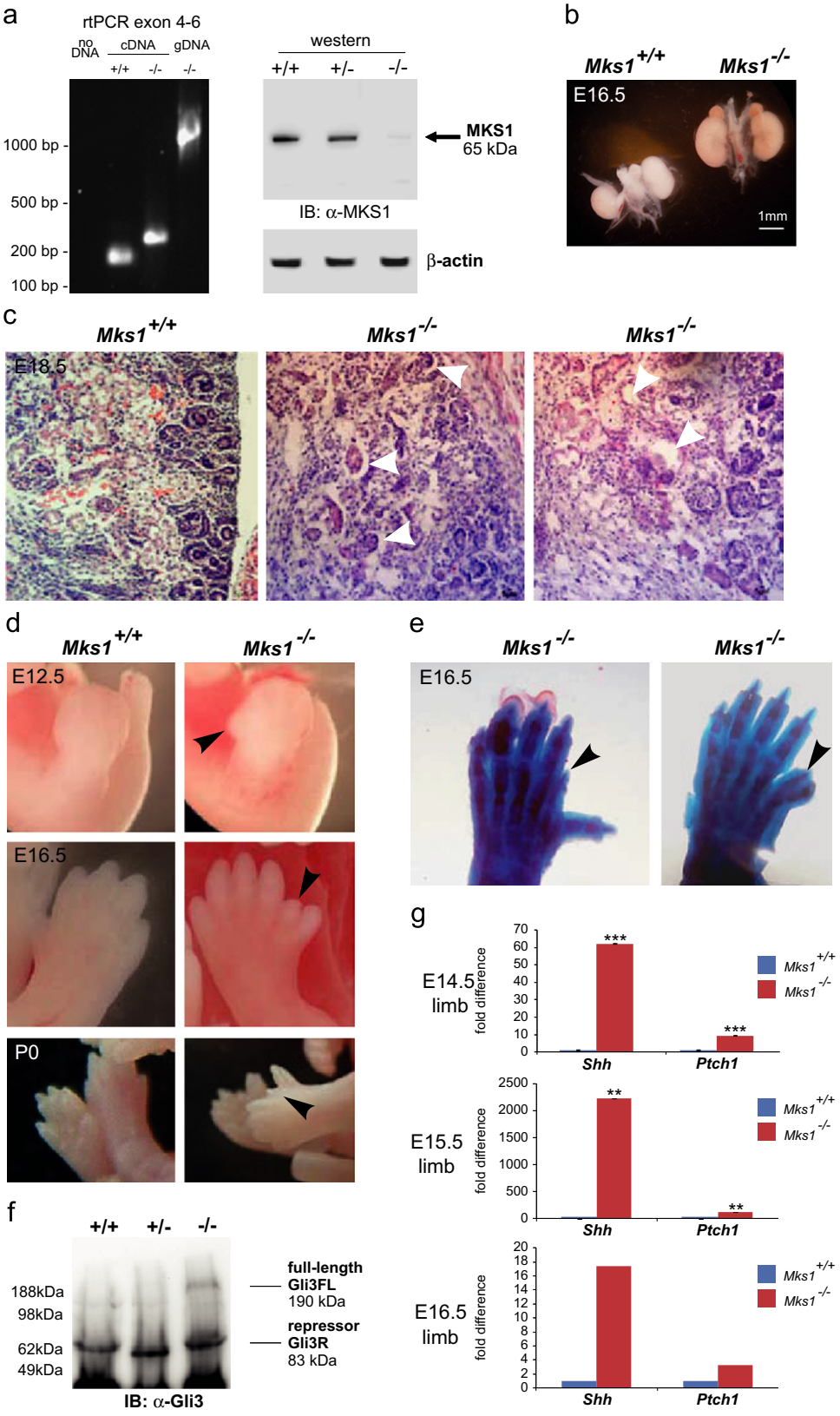

Fig. 1. (a) RT-PCR analysis of exons 4–6 in *Mks1*$^{+/+}$ and *Mks1*$^{-/-}$ MEFs, showing a larger PCR product in cDNA from mutant cells which Sanger sequencing shows to be due to insertion of the *tm1a* mutation cassette between exons 3 and 4. The mutation leads to almost total loss of Mks1 protein in the mutant animals, as shown by western blotting with an Mks1 antibody. Immunoblotting for β-actin is the loading control. (b) Enlarged kidneys in E16.5 *Mks1*$^{-/-}$ in comparison to *Mks1*$^{+/+}$ wild-type littermate. Scale bar=1 mm. (c) Glomerular microcysts in E18.5 *Mks1*$^{-/-}$ kidneys indicated by arrowheads. (d) Hind limb pre-axial polydactyly (arrowheads) at the indicated stages of development in *Mks1*$^{-/-}$ embryos. (e) Alcian blue and alizarin red staining of hind limbs in *Mks1*$^{-/-}$ animals showing variation in the polydactyly phenotype. Arrowheads point to the extra digit or part of digit. (f) Gli3 western blot showing increased levels of full-length Gli3 (Gli3FL) in comparison to Gli3 repressor (Gli3R) in *Mks1*$^{-/-}$ limb buds relative to *Mks1*$^{+/-}$ and *Mks1*$^{+/+}$. (g) Increased expression of *Shh* and Hh pathway target *Ptch1* (Patched 1) in E14.5, E15.5 and E16.5 limbs, as quantified by qRT-PCR. The graphs shows the fold difference in expression level of the two genes in *Mks1*$^{-/-}$ mutants compared to *Mks1*$^{+/+}$ wild-type littermate controls. Experiments were performed in triplicate ($n=3$) for E14.5 and E15.5 limb samples, and $n=2$ for E16.5 samples. The statistical significance of pair-wise comparisons for the expression of each gene (the $\Delta\Delta C_t$ value) in *Mks1*$^{+/+}$ and *Mks1*$^{-/-}$ E14.5 and E15.5 limbs are indicated ($^{**}p<0.01$, $^{***}p<0.001$). Error bars show the standard deviation of $\Delta\Delta C_t$.

Mks1 protein in cells. Western blot analysis of cell lysates from mouse embryonic fibroblasts (MEFs) confirmed that the *tm1a* allele was a strong hypomorph, with negligible levels of the Mks1 protein present in *Mks1*$^{-/-}$ cells compared to *Mks1*$^{+/+}$ *and* *Mks1*$^{+/-}$ controls (Fig. 1a).

Mks1$^{-/-}$ embryos survived to at least embryonic day E13.5 (n=20/20, 100%), but many then began to be resorbed (n=9/25 mutants, 24%), particularly as the line became more congenic ($F \geq 10$). However, a proportion of mutants (n=16/25, 76%) survived to later gestational ages, including P0, but were cyanotic in the immediate perinatal period and died by P1 presumably due to respiratory insufficiency.

Mutant *Mks1*$^{-/-}$ embryos had all of the expected features of a severe ciliopathy, including the hallmark MKS clinical features of renal cystic dysplasia, polydactyly and complex posterior fossa defects. Enlargement of the kidneys was seen from E16.5 (Fig. 1b) and small kidney cysts were observed in the glomerulus and cortex in mutant animals from E16.5 (Fig. 1c). This was only observed in 60% of mutants analysed, differing from the human condition for which the presence of cystic kidneys are an obligatory diagnostic feature. Pre-axial polydactyly was a consistent feature seen in all mutant embryos (n=35/35), but was observed only on the hind limbs (Fig. 1d). In some cases (n=4/35), the polydactyly was only obvious on one hind limb, but skeletal preparations of these animals showed the presence of an extra distal phalanx on the first digit (Fig. 1e). In contrast, human patients carrying MKS1 mutations usually have post-axial polydactyly, on both hands and feet (Khaddour et al., 2007). Polydactyly in the mutant mice was accompanied by an increase in levels of full-length Gli3 relative to the level of Gli3 repressor in mutant limb buds (Fig. 1f), which suggests disturbed Shh signalling activity similar to that seen in other severe ciliopathy mouse models with pre-axial polydactyly such as the *Ftm* mouse (Vierkotten et al., 2007). We confirmed that the expression of both *Shh* and *Ptch1* (*Patched 1*) genes, both downstream targets of the Hh pathway, was up-regulated in E14.5, E15.5 and E16.5 mutant limbs compared to wild-type or heterozygote littermates (Fig. 1g).

Mutant *Mks1*$^{-/-}$ embryos had a broad range of CNS malformations that included posterior fossa defects and hydrocephaly which was observed in the majority (n=32/35) of embryos (Fig. 2a). Enlargement of the fourth ventricle was often accompanied by cerebellar vermis hypoplasia, comprising the Dandy–Walker malformation (Fig. 2b). This defect was confirmed in all mutant brains suitable for analysis by sectioning (n=5/5). All animals had a reduced anterioposterior axis of the developing forebrain (Fig. 2c). Midline defects such as semilobar holoprosenchephaly, manifesting as poorly developed median longitudinal septum separating the cerebral hemispheres, consistent with defects in Shh signalling, and defective closure of the roof plate in the cranial neural tube were also observed (Fig. 2c). Other midline defects observed included enlarged fontanelles, incomplete closure of the occipital bones, enlargement and downward persistence of the aqueduct (Fig. 2d). Periventricular heterotopias were also commonly observed (Fig. 2e).

A number of additional features were observed in the *Mks1*$^{-/-}$ mice. Anophthalmia and microphthalmia were common features

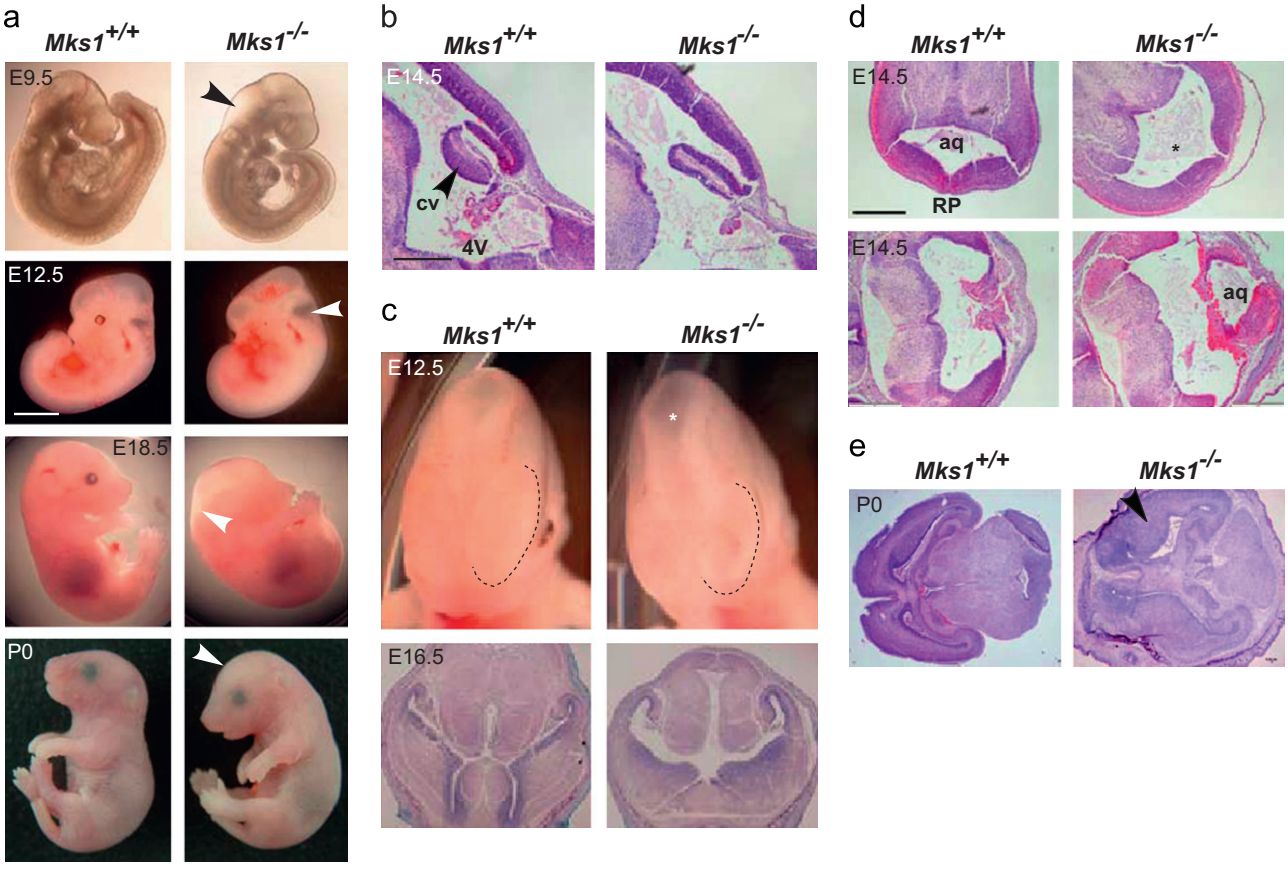

Fig. 2. (a) Hydrocephaly in *Mks1*$^{-/-}$ at the indicated stages of development. Arrowheads indicate cystic swelling of fourth ventricle in E9.5, 12.5 and 18.5 embryos and domed appearance of the front of the head in P0 pups. Anophthalmia can be seen in the E18.5 mutant embryo. (b) H&E stained midline sagittal sections of E14.5 hind brain in *Mks1*$^{-/-}$ and *Mks1*$^{+/+}$ littermates showing cystic swelling of fourth ventricle (4 V) and cerebellar vermis (cv) hypoplasia in the mutants, consistent with a Dandy–Walker malformation. (c) Small forebrain (dashed line) and defective closure of the roof plate in the cranial neural tube (asterisk) in E12.5 *Mks1*$^{-/-}$ animals compared to wild-type littermate controls. (d) H&E stained horizontal sections of E14.5 brains showing defective closure of roof plate (RP), downward placement of the aqueduct (aq) and swelling of the aqueduct and fourth ventricle (*). (e) H&E stained P0 horizontal brain sections showing periventricular heterotopias in *Mks1*$^{-/-}$ (arrowhead).

(n=10/35 and 21/35, respectively; Fig. 2a; Fig. 3a), as were lung hypoplasia and cardiomegaly, seen in all mutants analysed for these phenotypes (n=5/5) (Fig. 3b). Left–right patterning defects including left lung isomerism, dextrocardia, situs inversus and abnormal turning were common features in the mutants analysed (n=6/10; Fig. 3c). Craniofacial defects included micrognathia (n=7/35 mutants), cleft lip (n=4/35), hypertelorism (n=1/35), and dysmorphic ears (n=2/29) (Fig. 3d). Occasional features included bowing and shortening of the long bones (Fig. 3e), liver fibrosis and omphalocele.

To investigate the cell biology of this ciliopathy model, we derived mouse embryonic fibroblasts (MEFs) from E15.5 embryos. *Mks1*$^{-/-}$ MEFs had significant decreases in cilia number and cilia length compared to *Mks1*$^{+/+}$ MEFs, in addition to general disorganisation of the tubulin cytoskeleton (Fig. 4a). Immunofluorescence (IF) staining of cryosections confirmed a loss of cilia *in vivo* in ependymal cells of the developing neuroepithelium and in renal tubules for *Mks1*$^{-/-}$ E16.5 embryos (Fig. 4b). Further IF analysis of MEFs showed increased levels of nuclear β-catenin in *Mks1*$^{-/-}$ cells compared to *Mks1*$^{+/+}$ cells after stimulation of the canonical Wnt/β-catenin pathway with Wnt3a (Fig. 4c). Western blots showed a moderate increase in total levels of soluble β-catenin for *Mks1*$^{-/-}$ MEFs, as well as an increased level of cyclin D1, a downstream effector of the Wnt/β-catenin pathway (Fig. 4d). TOPFlash reporter assays of Wnt/β-catenin pathway activity confirmed statistically significant increases in both the basal levels of Wnt signalling and the levels following stimulation with Wnt3a in mutant fibroblasts (Fig. 4d). TOPFlash reporter assays further showed a statistically significant difference in Wnt signalling in mutant *Mks1*$^{-/-}$ MEFs and wild-type Mks1$^{+/+}$ MEFs after treatment with both Wnt3a and Wnt5a (Fig. 4d). However, activity was reduced by roughly 50% compared to treatment with Wnt3a only in both cell types, suggesting a similar response to Wnt5a in mutant and wild-type cells. Transient reverse transfection of siRNAs for *Mks1* into the ciliated cell-line IMCD3 also caused an increase in β-catenin levels in cells compared to scrambled control (Fig. 4e). *Mks1* knockdown caused a ciliogenesis defect compared to scrambled siRNA negative controls (Fig. 4e), as reported previously (Dawe et al., 2009) but also caused a statistically significant increase in cell number and cell proliferation which was not seen following knock-down of *Rpgrip1l*, a positive control for ciliogenesis (Fig. 4e).

To investigate the effects of canonical Wnt/β-catenin signalling defects on cell proliferation *in vivo*, we investigated IHC staining for the proliferation marker Ki-67 in *Mks1*$^{+/+}$ and *Mks1*$^{-/-}$ tissues. This revealed that cell proliferation levels were very high in the *Mks1*$^{-/-}$ cerebellar hemispheres and neocortex (Fig. 5a), suggesting that *in vivo* canonical Wnt signalling in these tissues was de-regulated at an earlier stage of gestation. A periventricular heterotopia also had high ectopic levels of cell proliferation. Neuronal cell proliferation in the wild-type *Mks1*$^{+/+}$ neocortex appeared to be restricted to the ventricular and subventricular zones. However, the mutant *Mks1*$^{-/-}$ neocortex was thinner, the lamination was disorganised without the formation of clear cortical plate, and cell proliferation was more diffuse throughout the tissue (Fig. 5a). This suggested that both neuronal proliferation and/or migration could be defective in the *Mks1*$^{-/-}$ neocortex. Concomitant with the increases with cell proliferation, IHC staining for the apoptosis marker active caspase 3 revealed increased levels of apoptosis in the cerebellar hemispheres of *Mks1*$^{-/-}$ E14.5 embryos (Fig. 5b).

In the developing kidney of *Mks1*$^{-/-}$ at E14.5 there was an overall increase in canonical Wnt/β-catenin signalling levels, compared to *Mks1*$^{+/+}$ animals, as measured by western blot for overall levels of β-catenin in the tissue and expression of the Wnt downstream target *Axin2* (Fig. 6a). Mutant and wild-type kidneys also had high levels of proliferation, as visualised by Ki-67 staining (Fig. 6b), with particularly high levels in proximal renal tubules at E14.5. This high level of proliferation persisted to E16.5 in the mutant kidney, when the first microcysts become apparent, at which stage there was a marked difference in levels of proliferation between *Mks1*$^{-/-}$ and *Mks1*$^{+/+}$ kidneys (Fig. 6b).

Discussion

MKS1 is thought to play a role in a number of signalling pathways. The involvement of MKS1 in the Shh signalling pathway has been described, with the detailed analysis of dorsoventral patterning defects in the caudal neural tube and polydactyly in the developing limb bud (Cui et al., 2011; Sang et al., 2011; Weatherbee et al., 2009). In the *Mks1*$^{tm1a(EUCOMM)Wtsi}$ mutants, we also observed increased levels of full-length Gli3, and increased expression of downstream targets of Shh signalling in embryonic limb-buds (Fig. 1f), consistent with the defective ciliogenesis in early *Mks1*$^{-/-}$ embryos (Fig. 4b). In the developing forebrain, disturbed Shh signalling is likely to cause the semilobar holoprosencephaly phenotype (Fig. 2c). However, the potential role of MKS1, a basal body protein, in regulating Wnt signalling has not been investigated previously, despite the manifestation of defects that were consistent with a defect in planar cell polarity (PCP) and non-canonical Wnt signalling in *Mks1*$^{del64\text{-}323}$ mutant mice (Cui et al., 2011). Furthermore, blastomeres in *mks1* morphant zebrafish show a convergent extension defect during embryogenesis, which are also typical of PCP non-canonical Wnt signalling defects (Leitch et al., 2008).

Our own data now show that MKS1 is required for correct ciliogenesis in the CNS and in MEFs. This ciliary phenotype directly correlated with de-regulation of Wnt/β-catenin signalling both *in vitro* (Fig. 4c–e) and *in vivo* (Fig. 6a), and is entirely consistent with previous reports that cilia act as negative regulators of the canonical Wnt/β-catenin signalling (Corbit et al., 2008; Gerdes et al., 2007; Lancaster et al., 2011b). In contrast to previous reports in other models, such as the *Ahi1* mouse that manifest milder ciliopathy features consistent with Joubert syndrome (JBTS) (Lancaster et al., 2011a), we do not see any evidence of abnormally long cilia or any failure to activate the canonical Wnt/β-catenin pathway. In the *Ahi1* model, the reduced canonical Wnt signalling accompanied reduced proliferation in the developing cerebellum (Lancaster et al., 2011a), whereas we observe much higher levels of proliferation in the cerebellum and cerebellar vermi of *Mks1* mutant embryos at mid-gestation (Fig. 5a). Despite increased levels of proliferation in the mutant animals, we observe hypoplasia of the cerebellar vermis. A reasonable hypothesis to test in future experiments is that this cerebellar hypoplasia in *Mks1* mutants is due to early de-regulation of Wnt/β-catenin signalling and cell over-proliferation in this tissue, followed by subsequent apoptosis. IHC staining for active caspase 3, an apotosis marker, in the cerebellum at E14.5 showed increased levels of expression in the mutant (Fig. 5b) and supported this hypothesis.

Wnt/β-catenin signalling seemed to be similarly de-regulated in the *Mks1* mutant kidney, since mutant kidneys had higher levels of *Axin2* expression than in wild-type littermates at E16.5 (Fig. 6a). We hypothesise that these Wnt/β-catenin signalling defects may contribute to the high proliferation rates in the mutant kidney to E16.5, when proliferation had slowed in the kidney of wild-type littermates (Fig. 6b). *Mks1*$^{-/-}$ embryos typically started to develop microcysts around this stage, presumably due to the high proliferation rates persisting in this tissue. It is not clear how this may be linked to de-regulated Wnt signalling in the mutant, but an increase in Wnt signalling earlier

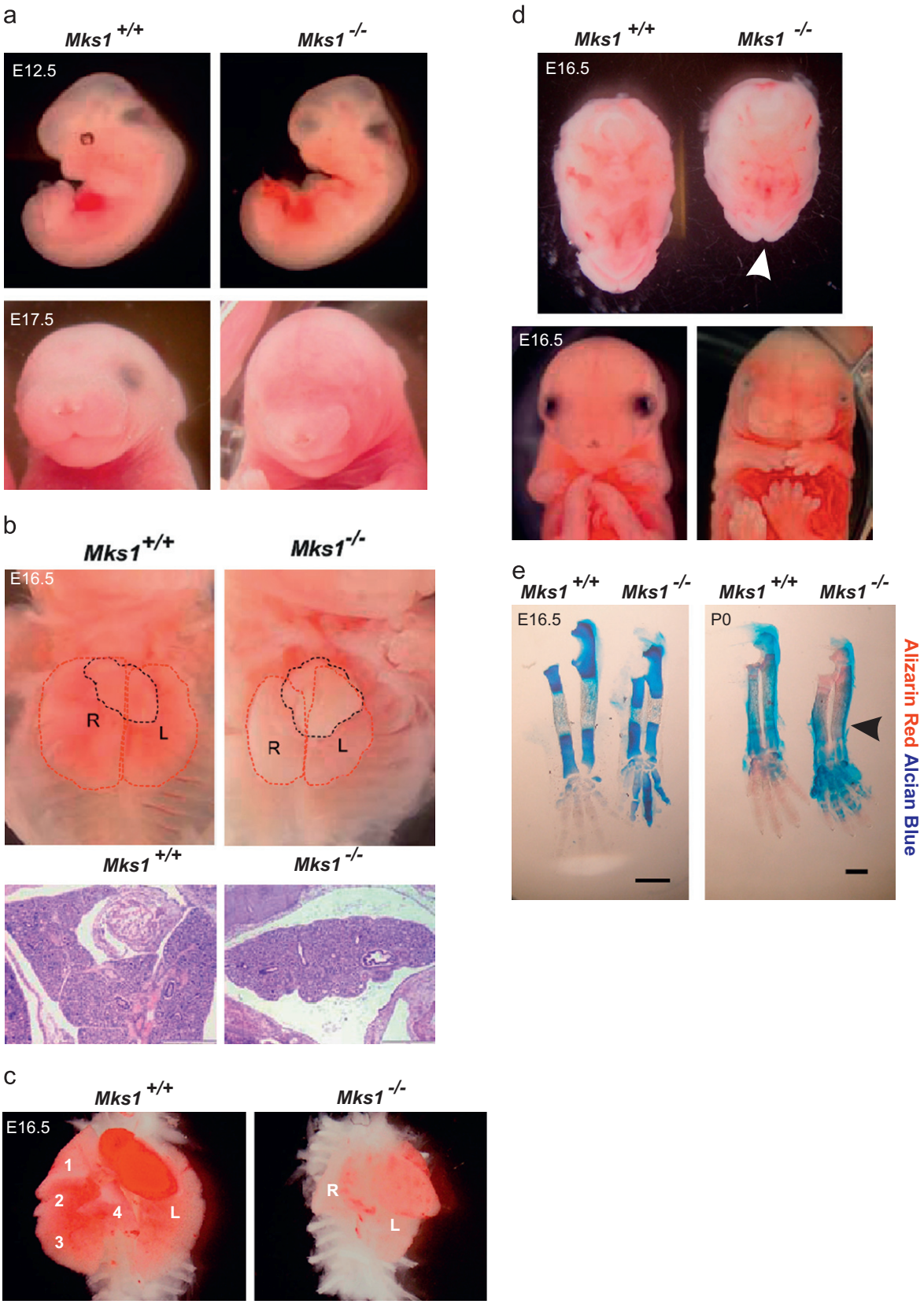

Fig. 3. (a) Microphthalmia in E12.5 *Mks1*$^{-/-}$ animal and anophthalmia in E17.5 mutant. (b) Upper panel: Whole mount showing lung hypoplasia and cardiomegaly in mutant E16.5 embryo compared to wild-type littermate. Lower panel: H&E stained sagittal sections of E16.5 thoracic cavity showing lung hypoplasia in *Mks1*$^{-/-}$. (c) Left pulmonary isomerism in mutant animal. The wild-type animal has one left lung with a single lobe and one right lung with four lobes, whereas the mutant has two single-lobed lungs. (d) Top panel: horizontal view of underside of E16.5 heads, showing microcephaly and cleft lip (arrowhead) in *Mks1*$^{-/-}$. Bottom panel: hypertelorism, microphthalmia and polydactyly in E16.5 *Mks1*$^{-/-}$ embryo. (e) Alizarin red and alcian blue staining of bone and cartilage, showing bowing (arrowhead) and shortening of the long bones in *Mks1*$^{-/-}$ E16.5 and P0 pups.

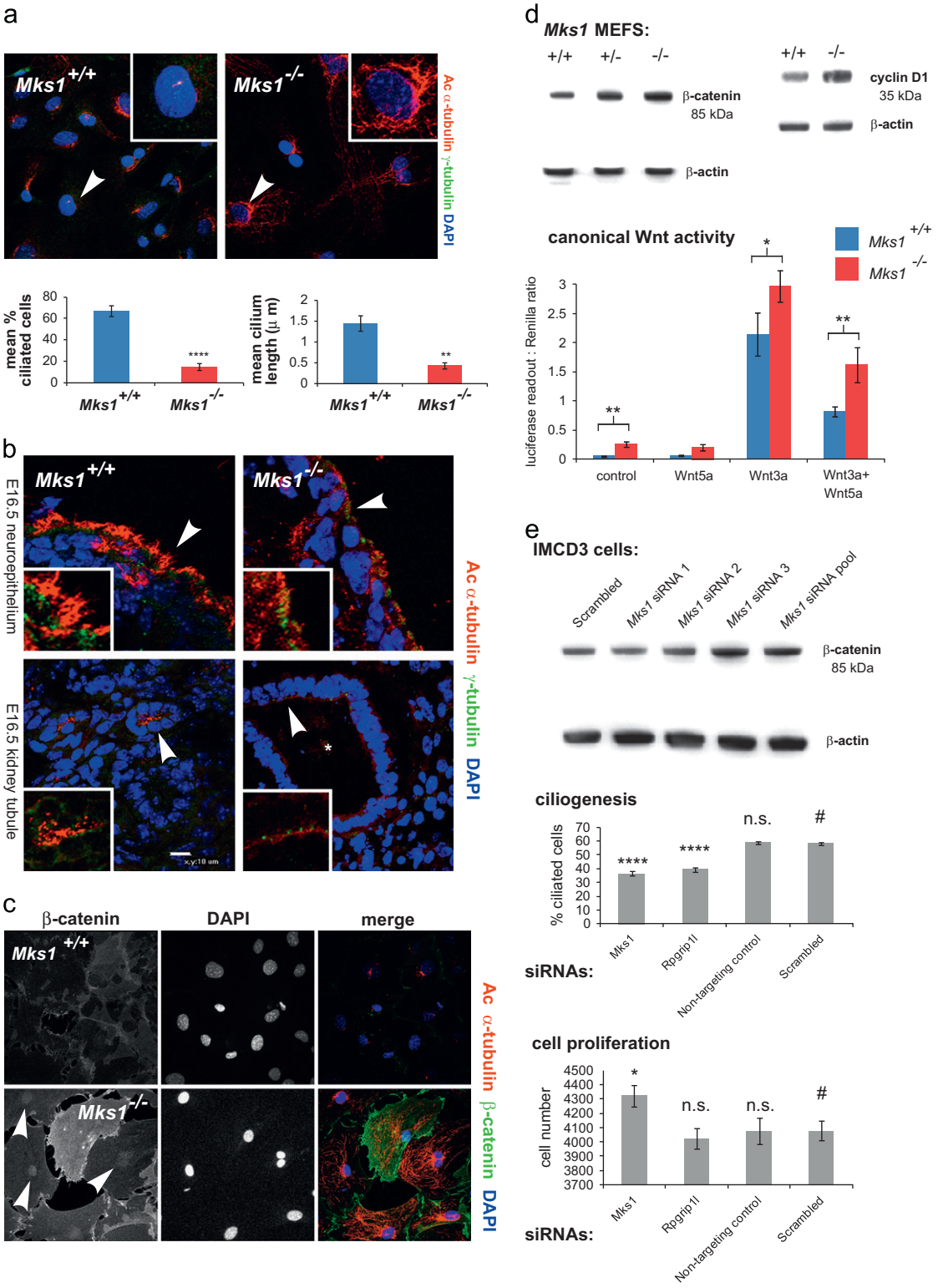

Fig. 4. (a) Immunofluorescence (IF) staining of *Mks1* MEFs, showing cilia stained with acetylated alpha-tubulin antibody, basal bodies stained with gamma-tubulin antibody and nuclei stained with DAPI. Graphs show statistical significance of pair-wise comparisons of number and cilia length between $Mks1^{-/-}$ and $Mks1^{+/+}$ cells (**$p < 0.01$, ****$p < 0.0001$). Error bars indicate s.e.m. (b) IF staining of E16.5 *Mks1* sagittal cryosections, showing cilia stained with acetylated alpha tubulin in ependymal cells of the developing neuroepithelium (arrowhead; upper panel) and epithelial cells of proximal renal tubules (arrowhead; bottom panel). $Mks1^{-/-}$ mutants have lost cilia on neuroepithelial cells (arrowhead) and in an expanded renal tubule (asterisk). (c) IF staining of *Mks1* MEFs showing increased levels of nuclear β-catenin in $Mks1^{-/-}$ cells compared to $Mks1^{+/+}$ cells after stimulation of the canonical Wnt/β-catenin pathway with Wnt3a. (d) Western blots showing a moderate increase in total levels of soluble β-catenin in $Mks1^{-/-}$ MEFs, as well as an increased level of cyclin D1. Immunoblotting for β-actin shows equal loading. Graph showing Firefly luciferase readout normalised against Renilla luciferase transfection control in *Mks1* MEFs after treatment with various conditioned media. There are statistically significant increases (*$p < 0.05$ **$p < 0.01$ for the indicated pair-wise comparisons)) in both the basal levels of Wnt signalling and the levels following stimulation with Wnt3a in mutant fibroblasts. Error bars indicate s.e.m., with assays performed in triplicate. (e) Increase in β-catenin levels after *Mks1* knockdown compared to scrambled negative control in IMCD3 cells. β-actin loading control shown below. Graphs showing percentage ciliated cells and cell number after transient reverse transfection of siRNAs into the ciliated cell-line IMCD3. *Mks1* and *Rpgrip1l* knockdowns had significant effects on levels of ciliogenesis. *Mks1* knockdown also had a significant effect on cell number and cell proliferation which was not seen following knock-down of *Rpgrip1l* or a non-targeting control. Statistical significance of the indicated pair-wise comparisons against the negative control (#) are shown (n.s. not significant; *$p > 0.05$; ****$p > 0.0001$). Error bars indicate s.e.m.

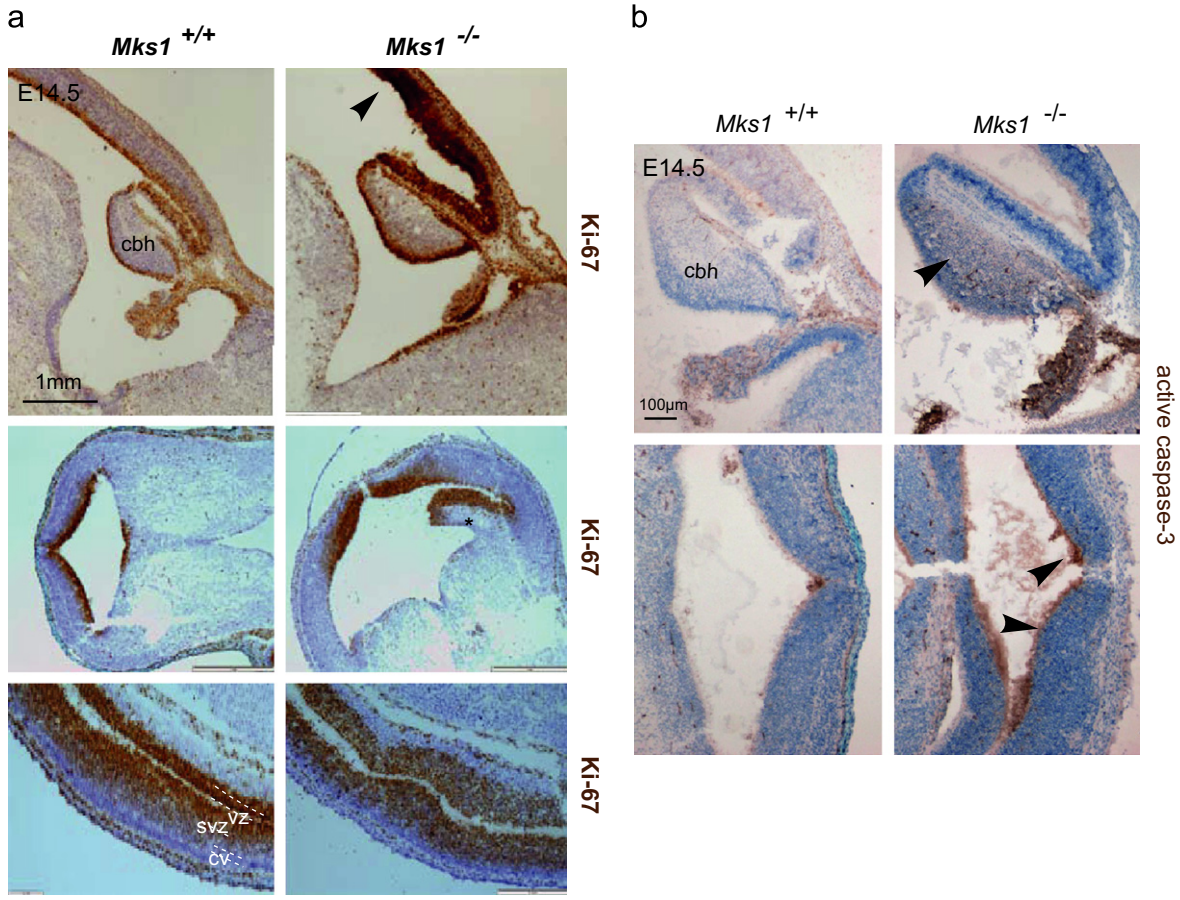

Fig. 5. (a) Immunohistochemical (IHC) staining of E14.5 brain sections of *Mks1* embryos with Ki-67 antibody, a proliferation marker, and counterstained with haematoxylin. Upper panel: approximately midline sagittal section showing cerebellar hemispheres (cbh), with high levels of neuronal proliferation in the neocortex indicated by the arrowhead. Middle panel: horizontal section of hind brain region, including heterotopia (asterisk) in the mutant. Bottom panel: horizontal section of cerebral cortex and lateral ventricles, with lamination of the wild-type $Mks1^{+/+}$ neocortex indicated (vz, ventricular zone; svz, sub-venricular zone and cv, cortical plate). Note the loss of lamination in the $Mks1^{-/-}$ mutant. Scale bar = 1 mm. (b) E14.5 brain sections, comparable to those shown in (a), IHC stained with active caspase 3 antibody, an apoptosis marker, and counterstained with haematoxylin. Upper panel: approximately midline sagittal section showing cerebellar hemispheres (cbh), with increased levels of apoptosis in the $Mks1^{-/-}$ mutant indicated by the arrowhead. Bottom panel: horizontal section of hind brain region, showing increased apoptosis in the cerebellum of the mutant (arrowheads). Scale bar = 100 μm.

in gestation (prior to E14.5) may lead to the increased proliferation later in development.

The role of MKS1 in the mTOR pathway and cell proliferation has also been suggested, based on experiments with rapamycin, a small molecule inhibitor of the mTOR pathway which has been shown to slow progression of polycystic kidney disease (PKD) in rat models of the disease (Tao et al., 2005). Treatment of *mks1* morphant zebrafish embryos with 10 nM rapamycin in tank water 24 h after morpholinooligonucleotide (MO) microinjection has been shown to rescue 75% of morphant embryos. Partial amelioration of the kidney phenotype in *mks1* morphant embryos was also seen after treatment with roscovitine, an inhibitor of a cyclin dependent kinase, which has been shown to successfully reduce cyst growth in mice with PKD (Bukanov et al., 2006). These results suggest possible therapeutic potential for treatment of severe ciliopathies that manifest renal cystic dysplasia (Tobin and Beales, 2008). A role of MKS1 in the downstream regulation of the mTOR pathway is entirely consistent with our data which suggests a role for MKS1 in regulating cell proliferation. We observed increased proliferation *in vitro* following siRNA knockdown (Fig. 4e) and increased levels of cyclin D1 in mutant MEFs (Fig. 4d). *In vivo*, both the developing brain and kidney early in gestation had high ectopic levels of cell proliferation in mutant embryos (Figs. 5a, 6b). In contrast, knockdown of another ciliopathy gene, *Rpgrip1l*, had no effect on cell proliferation (Fig. 4e), which suggests that this function is gene- and perhaps even context-specific. The potential role of the primary cilium in regulating the cell cycle is a topical subject of discussion (Jackson, 2011), with the suggestion that the cilium is a 'tumour suppressor organelle' (Mans et al., 2008). It is interesting to note that IFT88 (known previously as Tg737) and which is now known to mediate intraflagellar transport along the ciliary axoneme, has also been characterised as a putative tumour suppressor gene (Isfort et al., 1997).

There is much phenotypic variation within MKS, including intrafamilial and inter-individual variability. In a study of multiplex MKS families in which the proband had the classical triad of MKS symptoms, only 68% of affected siblings were also diagnosed with MKS (Fraser and Lytwyn, 1981). Occipital encephalocele and post-axial polydactyly have a more variable presentation than cystic kidney dysplasia, with some of this variation in phenotype correlated to the genotype of the affected individual. Mutations in *MKS1* are almost always associated with polydactyly and occipital encephalocele: in one study all MKS1 patients had the classic triad of MKS symptoms with the addition of hepatic ductal dysplasia (Auber et al., 2007). This can be contrasted with *MKS3*-mutated patients, which show lower incidence of polydactyly and CNS malformations (Consugar et al., 2007). Mutations in *MKS3* can also cause the milder

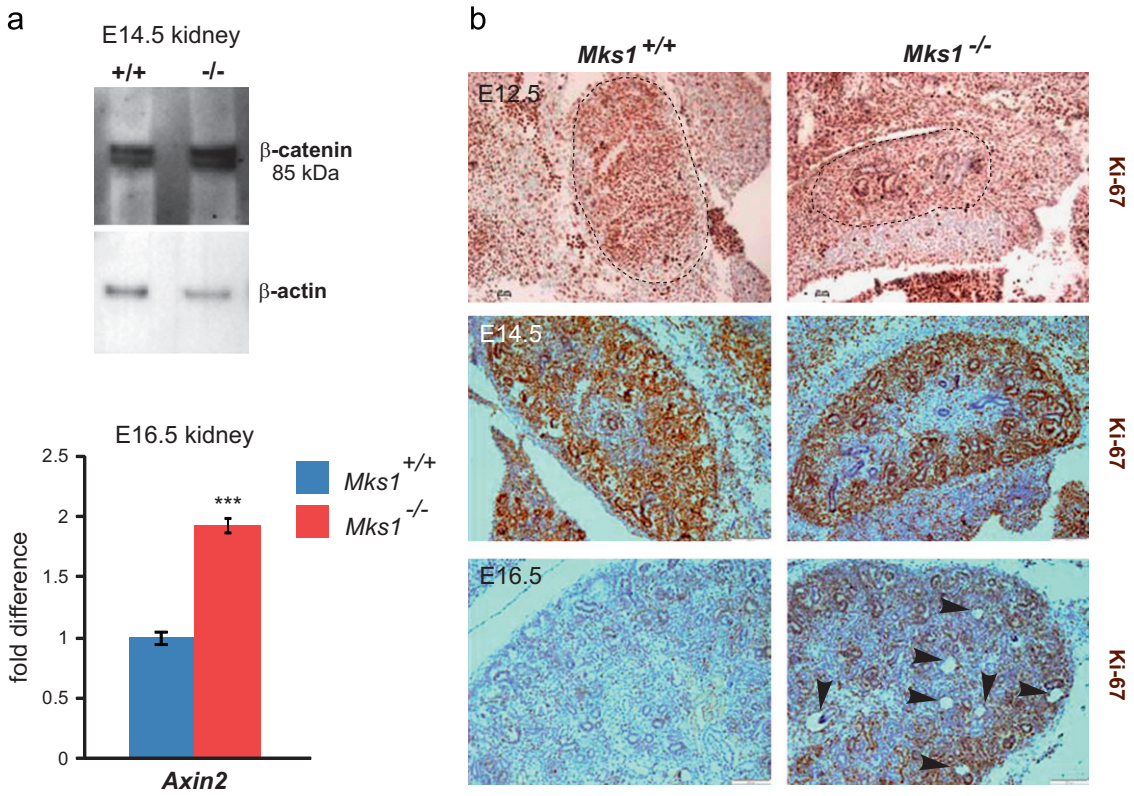

Fig. 6. (a) Top panel: Western blot showing increased levels of total β-catenin in E14.5 kidneys in *Mks1*$^{-/-}$ mutants (−/−) compared to wild-type (+/+) littermates. Bottom panel: increased expression of Wnt pathway target *Axin2* in E16.5 kidney, as quantified by qRT-PCR. The graph shows the fold difference in expression level in *Mks1*$^{-/-}$ mutants compared to *Mks1*$^{+/+}$ wild-type littermate control kidney tissue performed in triplicate ($n=3$). The statistical significance of the pair-wise comparison is indicated (**$p < 0.001$). Error bars show the standard deviation of $\Delta\Delta C_t$. (b) Sagittal kidney sections at E12.5 (top panel), E14.5 (middle panel) and E16.5 (bottom panel), stained with Ki67 antibody and counterstained with haematoxylin. Dashed lines outline the kidney in each section. Arrowheads indicate microcysts.

neurodevelopmental condition Joubert syndrome (JBTS) (Baala et al., 2007), and there are frequent instances of intrafamilial variation in the expressivity of the MKS and JBTS phenotypes (Smith et al., 2006). In another study, 5 out of 12 *MKS1*-mutated cases were found to have bone dysplasia and cleft palate, and two of the 12 showed *situs inversus* (Khaddour et al., 2007). However, to date, *MKS1* mutations have not been found as causative for JBTS which suggests that phenotypic variability is limited to the severe, MKS range of the disease spectrum.

Although we observed some phenotypic variation including intra-individual variation in the congenic *Mks1* line, we did not observe the highly variable range of phenotypes seen for the congenic *Tmem67/Mks3* knock-out mouse which recapitulated the human disease spectrum from MKS to JBTS (Abdelhamed et al., in press). In this, the restricted and severe phenotype of *Mks1* mutant embryos also recapitulated the MKS phenotype of *MKS1*-mutated patients. In particular, polydactyly is seen as an almost obligatory feature of *MKS1*-mutated patients in humans, but is far less common in *MKS3*-mutated patients. This pattern is seen in the mice, with 100% of *Mks1* mutants showing polydactyly, and a total absence of this feature in *Tmem67* mice. MKS type 1 human patients often have more severe phenotypes than MKS type 3 patients, and this is also recapitulated in the mouse models: *Mks1* mutants have severe developmental defects and often die at E13.5, whereas *Tmem67/Mks3* mutants usually develop sufficiently to allow survival to P0 and die at birth of respiratory insufficiency. We therefore conclude that the *Mks1*$^{tm1a(EUCOMM)Wtsi}$ line fully recapitulates not only human MKS type 1, but also the severe and restricted nature of this specific ciliopathy phenotype.

The high degree of congenicity in both our *Tmem67* and *Mks1* lines ($F > 10$ generations) would argue against the modifier allele hypothesis (Zaki et al., 2011) which would otherwise provide an attractive explanation for the unexpected phenotypic variability in *Tmem67*$^{-/-}$ embryos. Instead, we speculate that the signalling cascades mediated by MKS1 from the primary cilium are resistant to the effect of environmental factors on inter-individual levels of gene expression, whereas those mediated by TMEM67 are more susceptible. It will be particularly interesting to determine the molecular mechanisms that lead to a broad ciliopathy phenotype if TMEM67 is lost in both humans and mice, but a restricted, more severe phenotype if MKS1 is lost.

Acknowledgements

We thank A. Monk, K. Passam and T. Simpson of Nikon UK Ltd. for technical support and advice on confocal microscopy. We are very grateful to D. Evans, J. Bilton, C. McCartney and M. Reay for technical support. We thank R. T. Moon, University of Washington, for the TOPFlash and FOPFlash constructs. The anti-Gli3 antibody was the kind gift of S. Scales, Genentech, *CA*, USA. We acknowledge funding from the UK Medical Research Council (GW, Doctoral Training Award; CAJ, project grant G0700073) and an Egyptian Government Scholarship (ZA). The research also received funding from the European Community's Seventh Framework Programme FP7/2009 under grant agreement no: 241955 SYSCILIA. The funders had no role in study design, data collection and analysis, decision to publish, or preparation of the manuscript.

References

Abdelhamed, Z., Wheway, G., Szymanska, K., Natarajan, S., Toomes, C., Inglehearn, C., Johnson, C.A. Variable expressivity of ciliopathy neurological phenotypes that encompass Meckel–Gruber syndrome and Joubert syndrome is caused by complex de-regulated ciliogenesis, Shh and Wnt signalling defects. Hum. Mol. Genet. http://dx.doi.org/10.1093/hmg/dds546, in press.

Adams, M., Smith, U.M., Logan, C.V., Johnson, C.A., 2008. Recent advances in the molecular pathology, cell biology and genetics of ciliopathies. J. Med. Genet. 45, 257–267.

Ahdabbarmada, M., Claassen, D., 1990. A distinctive triad of malformations of the central-nervous-system in the Meckel–Gruber syndrome. J. Neuropathol. Exp. Neurol. 49, 610–620.

Auber, B., Burfeind, P., Herold, S., Schoner, K., Simson, G., Rauskolb, R., Rehder, H., 2007. A disease causing deletion of 29 base pairs in intron 15 in the MKS1 gene is highly associated with the campomelic variant of the Meckel–Gruber syndrome. Clin. Genet. 72, 454–459.

Baala, L., Romano, S., Khaddour, R., Saunier, S., Smith, U.M., Audollent, S., Ozilou, C., Faivre, L., Laurent, N., Foliguet, B., Munnich, A., Lyonnet, S., Salomon, R., Encha-Razavi, F., Gubler, M.-C., Boddaert, N., de Lonlay, P., Johnson, C.A., Vekemans, M., Antignac, C., Attié-Bitach, T., 2007. The Meckel–Gruber syndrome gene, MKS3, is mutated in Joubert syndrome. Am. J. Hum. Genet. 80, 186–194.

Bukanov, N.O., Smith, L.A., Klinger, K.W., Ledbetter, S.R., Ibraghimov-Beskrovnaya, O., 2006. Long-lasting arrest of murine polycystic kidney disease with CDK inhibitor roscovitine. Nature 444, 949–952.

Consugar, M., Kubly, V., Lager, D., Hommerding, C., Wong, W., Bakker, E., Gattone, V., Torres, V., Breuning, M., Harris, P., 2007. Molecular diagnostics of Meckel–Gruber syndrome highlights phenotypic differences between MKS1 and MKS3. Hum. Genet. 121, 591–599.

Corbit, K.C., Shyer, A.E., Dowdle, W.E., Gaulden, J., Singla, V., Reiter, J.F., 2008. Kif3a constrains [beta]-catenin-dependent Wnt signalling through dual ciliary and non-ciliary mechanisms. Nat. Cell Biol. 10, 70–76.

Cui, C., Chatterjee, B., Francis, D., Yu, Q., SanAgustin, J.T., Francis, R., Tansey, T., Henry, C., Wang, B., Lemley, B., Pazour, G.J., Lo, C.W., 2011. Disruption of Mks1 localization to the mother centriole causes cilia defects and developmental malformations in Meckel–Gruber syndrome. Dis. Models Mechan. 4, 43–56.

Dandy, W.E., Blackfan, K.D., 1914. Internal hydrocephalus—an experimental, clinical and pathological study. Am. J. Dis. Child. 8, 406–482.

Davis, E.E., Brueckner, M., Katsanis, N., 2006. The emerging complexity of the vertebrate cilium: new functional roles for an ancient organelle. Dev. Cell 11, 9–19.

Dawe, H.R., Adams, M., Wheway, G., Szymanska, K., Logan, C.V., Noegel, A.A., Gull, K., Johnson, C.A., 2009. Nesprin-2 interacts with meckelin and mediates ciliogenesis via remodelling of the actin cytoskeleton. J. Cell Sci. 122, 2716–2726.

Dawe, H.R., Smith, U.M., Cullinane, A.R., Gerrelli, D., Cox, P., Badano, J.L., Blair-Reid, S., Sriram, N., Katsanis, N., Attie-Bitach, T., Afford, S.C., Copp, A.J., Kelly, D.A., Gull, K., Johnson, C.A., 2007a. The Meckel–Gruber Syndrome proteins MKS1 and meckelin interact and are required for primary cilium formation. Hum. Mol. Genet. 16, 173–186.

Dawe, H.R., Smith, U.M., Cullinane, A.R., Gerrelli, D., Cox, P., Badano, J.L., Blair-Reid, S., Sriram, N., Katsanis, N., Attie-Bitach, T., Afford, S.C., Copp, A.J., Kelly, D.A., Gull, K., Johnson, C.A., 2007b. The Meckel–Gruber syndrome proteins MKS1 and meckelin interact and are required for primary cilium formation. Hum. Mol. Genet. 16, 173–186.

Elmehdawi, F., Wheway, G., Szymanska, K., Adams, M., High, A.S., Johnson, C.A., Robinson, P.A., 2013. Human Homologue of Drosophila Ariadne (HHARI) is a marker of cellular proliferation associated with nuclear bodies. Exp. Cell Res. 319, 161–172.

Fraser, F.C., Lytwyn, A., 1981. Spectrum of anomalies in the Meckel syndrome, or maybe there is a malformation syndrome with at least one constant anomaly. Am. J. Med. Genet. 9, 67–73.

Garcia-Gonzalo, F.R., Corbit, K.C., Sirerol-Piquer, M.S., Ramaswami, G., Otto, E.A., Noriega, T.R., Seol, A.D., Robinson, J.F., Bennett, C.L., Josifova, D.J., Garcia-Verdugo, J.M., Katsanis, N., Hildebrandt, F., Reiter, J.F., 2011. A transition zone complex regulates mammalian ciliogenesis and ciliary membrane composition. Nat. Genet. 43, 776–784.

Genuardi, M., Dionisivici, C., Sabetta, G., Mignozzi, M., Rizzoni, G., Cotugno, G., Neri, M.E.M., 1993. Cerebro-reno-digital (Meckel-like) syndrome with Dandy–Walker malformation, cystic kidneys, hepatic fibrosis and polydactyly. Am. J. Med. Genet. 47, 50–53.

Gerdes, J.M., Liu, Y., Zaghloul, N.A., Leitch, C.C., Lawson, S.S., Kato, M., Beachy, P.A., Beales, P.L., DeMartino, G.N., Fisher, S., Badano, J.L., Katsanis, N., 2007. Disruption of the basal body compromises proteasomal function and perturbs intracellular Wnt response. Nat. Genet. 39, 1350–1360.

Herriot, R., Hallam, L.A., Gray, E.S., 1991. Dandy–Walker malformation in the Meckel syndrome American. J. Med. Genet. 39, 207–210.

Isfort, R.J., Cody, D.B., Doersen, C.J., Richards, W.G., Yoder, B.K., Wilkinson, J.E., Kier, L.D., Jirtle, R.L., Isenberg, J.S., Klounig, J.E., Woychik, R.P., 1997. The tetratricopeptide repeat containing Tg737 gene is a liver neoplasia tumor suppressor gene. Oncogene 15, 1797–1803.

Jackson, P.K., 2011. Do cilia put brakes on the cell cycle? Nat. Cell Biol. 13, 340–342.

Khaddour, R., Smith, U., Baala, L., Martinovic, J., Clavering, D., Shaffiq, R., Ozilou, C., Cullinane, A., Kyttala, M., Shalev, S., Audollent, S., d'Humieres, C., Kadhom, N., Esculpavit, C.P., Viot, G., Boone, C., Oien, C., Encha-Razavi, F., Batman, P.A., Bennett, C.P., Woods, C.G., Roume, J., Lyonnet, S., Genin, E., Le Merrer, M., Munnich, A., Gubler, M.-C., Cox, P., Macdonald, F., Vekemans, M., Johnson, C.A., Attie-Bitach, T., Soffoet, 2007. Spectrum of MKS1 and MKS3 mutations in Meckel syndrome: a genotype-phenotype correlation. Mutation in brief #960. Online. Hum. Mutat. 28, 523–524.

Kyttala, M., Tallila, J., Salonen, R., Kopra, O., Kohlschmidt, N., Paavola-Sakki, P., Peltonen, L., Kestila, M., 2006. MKS1, encoding a component of the flagellar apparatus basal body proteome, is mutated in Meckel syndrome. Nat. Genet. 38, 155–157.

Lancaster, M.A., Gopal, D.J., Kim, J., Saleem, S.N., Silhavy, J.L., Louie, C.M., Thacker, B.E., Williams, Y., Zaki, M.S., Gleeson, J.G., 2011a. Defective Wnt-dependent cerebellar midline fusion in a mouse model of Joubert syndrome. Nat. Med. 17, 726–731.

Lancaster, M.A., Schroth, J., Gleeson, J.G., 2011b. Subcellular spatial regulation of canonical Wnt signalling at the primary cilium. Nat. Cell Biol. 13, 700–707.

Leitch, C.C., Zaghloul, N.A., Davis, E.E., Stoetzel, C., Diaz-Font, A., Rix, S., Alfadhel, M., Lewis, R.A., Eyaid, W., Banin, E., Dollfus, H., Beales, P.L., Badano, J.L., Katsanis, N., 2008. Hypomorphic mutations in syndromic encephalocele genes are associated with Bardet–Biedl syndrome. Nat. Genet. 40, 443–448.

Lowry, R.B., Hill, R.H., Tischler, B., 1983. Survival and spectrum of anomalies in the meckel syndrome. Am. J. Med. Genet. 14, 417–421.

Mans, D.A., Voest, E.E., Giles, R.H., 2008. All along the watchtower: is the cilium a tumor suppressor organelle? Biochim. Biophys. Acta Rev. Cancer 1786, 114–125.

Moerman, P., Verbeken, E., Fryns, J.P., Goddeeris, P., Lauweryns, J.M., 1982a. Association of Meckel syndrome with m-anisosplenia in one patient. Clin. Genet. 22, 143–147.

Moerman, P., Verbeken, E., Fryns, J.P., Goddeeris, P., Lauweryns, J.M., 1982b. The Meckel syndrome—pathological and cytogenetic observations in 8 cases. Hum. Genet. 62, 240–245.

Murray, J.C., Johnson, J.A., Bird, T.D., 1985. Dandy–Walker malformation—etiologic heterogeneity and empiric recurrence risks. Clin. Genet. 28, 272–283.

Nagy, A., Gertsenstein, M., Vintersten, K., Behringer, R., 2003. Manipulating the Mouse Embryo, A Laboratory Manual, 3rd ed. Cold Spring Harbor Laboratory Press, New York.

Nauli, S.M., Alenghat, F.J., Luo, Y., Williams, E., Vassilev, P., Li, X., Elia, A.E.H., Lu, W., Brown, E.M., Quinn, S.J., Ingber, D.E., Zhou, J., 2003. Polycystins 1 and 2 mediate mechanosensation in the primary cilium of kidney cells. Nat. Genet. 33, 129–137.

Nonaka, S., Tanaka, Y., Okada, Y., Takeda, S., Harada, A., Kanai, Y., Kido, M., Hirokawa, N., 1998. Randomization of left–right asymmetry due to loss of nodal cilia generating leftward flow of extraembryonic fluid in mice lacking KIF3B motor protein. Cell 95, 829–837.

Paetau, A., Salonen, R., Haltia, M., 1985. Brain pathology in the Meckel syndrome—a study of 59 cases. Clin. Neuropathol. 4, 56–62.

Praetorius, H.A., Spring, K.R., 2001. Bending the MDCK cell primary cilium increases intracellular calcium. J. Membr. Biol. 184, 71–79.

Rapola, J., Salonen, R., 1985. Visceral anomalies in the Meckel syndrome. Teratology 31, 193–201.

Salonen, R., 1984. The Meckel syndrome—clinicopathological findings in 67 patients. Am. J. Med. Genet. 18, 671–689.

Sang, L.Y., Miller, J.J., Corbit, K.C., Giles, R.H., Brauer, M.J., Otto, E.A., Baye, L.M., Wen, X.H., Scales, S.J., Kwong, M., Huntzicker, E.G., Sfakianos, M.K., Sandoval, W., Bazan, J.F., Kulkarni, P., Garcia-Gonzalo, F.R., Seol, A.D., O'Toole, J.F., Held, S., Reutter, H.M., Lane, W.S., Rafiq, M.A., Noor, A., Ansar, M., Devi, A.R.R., Sheffield, V.C., Slusarski, D.C., Vincent, J.B., Doherty, D.A., Hildebrandt, F., Reiter, J.F., Jackson, P.K., 2011. Mapping the NPHP-JBTS-MKS protein network reveals ciliopathy disease genes and pathways. Cell 145, 513–528.

Simpson, J., Mills, J., Rhoads, G.G., Cunningham, G.C., Conley, M.R., Hoffman, H.J., 1991. Genetic heterogeneity in neural tube defects. Ann. Genet. 34, 7.

Smith, U.M., Consugar, M., Tee, L.J., McKee, B.M., Maina, E.N., Whelan, S., Morgan, N.V., Goranson, E., Gissen, P., Lilliquist, S., Aligianis, I.A., Ward, C.J., Pasha, S., Punyashthiti, R., Malik Sharif, S., Batman, P.A., Bennett, C.P., Woods, C.G., McKeown, C., Bucourt, M., Miller, C.A., Cox, P., AlGazali, L., Trembath, R.C., Torres, V.E., Attie-Bitach, T., Kelly, D.A., Maher, E.R., Gattone, V.H., Harris, P.C., Johnson, C.A., 2006. The transmembrane protein meckelin (MKS3) is mutated in Meckel–Gruber syndrome and the wpk rat. Nat. Genet. 38, 191–196.

Sugiura, Y., Suzuki, Y., Kobayashi, M., 1996. The Meckel syndrome: report of two Japanese sibs and a review of literature. Am. J. Med. Genet. 67, 312–314.

Summers, M.C., Donnenfeld, A.E., 1995. Dandy–Walker malformation in the Meckel syndrome. Am. J. Med. Genet. 55, 57–61.

Taggart, J.K., Walker, A.E., 1942. Congenital atresia of the foramens of Luschka and Magendie. Arch. Neurol. Psychiatry 48, 583–612.

Tao, Y.X., Kim, J., Schrier, R.W., Edelstein, C.L., 2005. Rapamycin markedly slows disease progression in a rat model of polycystic kidney disease. J. Am. Soc. Nephrol. 16, 46–51.

Tobin, J.L., Beales, P.L., 2008. Restoration of renal function in zebrafish models of ciliopathies. Pediatr. Nephrol. 23, 2095–2099.

Vierkotten, J., Dildrop, R., Peters, T., Wang, B.L., Ruther, U., 2007. Ftm is a novel basal body protein of cilia involved in Shh signalling. Development 134, 2569–2577.

Weatherbee, S.D., Niswander, L.A., Anderson, K.V., 2009. A mouse model for Meckel syndrome reveals Mks1 is required for ciliogenesis and Hedgehog signalling. Hum. Mol. Genet. 18, 4565–4575.

Wen, X.H., Lai, C.K., Evangelista, M., Hongo, J.A., de Sauvage, F.J., Scales, S.J., 2010. Kinetics of Hedgehog-dependent full-length Gli3 accumulation in primary cilia and subsequent degradation. Mol. Cell Biol. 30, 1910–1922.
Willert, K., Brown, J.D., Danenberg, E., Duncan, A.W., Weissman, I.L., Reya, T., Yates, J.R., Nusse, R., 2003. Wnt proteins are lipid-modified and can act as stem cell growth factors. Nature 423, 448–452.
Williams, C.L., Winkelbauer, M.E., Schafer, J.C., Michaud, E.J., Yoder, B.K., 2008. Functional redundancy of the B9 proteins and nephrocystins in Caenorhabditis elegans ciliogenesis. Mol. Biol. Cell 19, 2154–2168.
Xu, J., 2001. Preparation, Culture, and Immortalization of Mouse Embryonic Fibroblasts, Current Protocols in Molecular Biology. John Wiley & Sons, Inc. http://dx.doi.org/10.1002/0471142727.mb2801s70.
Zaki, M.S., Sattar, S., Massoudi, R.A., Gleeson, J.G., 2011. Co-occurrence of distinct ciliopathy diseases in single families suggests genetic modifiers. Am. J. Med. Genet. A 155, 3042–3049.